

# Dynamic Nuclear Polarization NMR Spectroscopy of Microcrystalline Solids

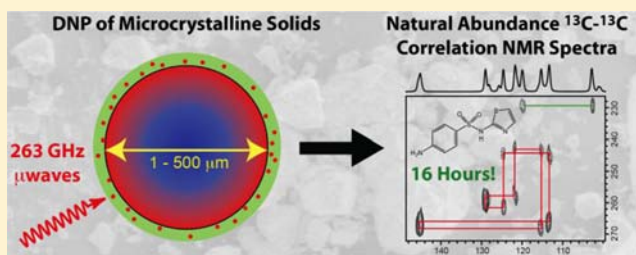
Aaron J. Rossini,<sup>†</sup> Alexandre Zagdoun,<sup>†</sup> Franziska Hegner,<sup>†</sup> Martin Schwarzwälder,<sup>‡</sup> David Gajan,<sup>†</sup> Christophe Copéret,<sup>‡</sup> Anne Lesage,<sup>†</sup> and Lyndon Emsley<sup>\*,†</sup>

<sup>†</sup>Centre de RMN a Tres Hauts Champs, Université de Lyon (CNRS/ENS Lyon/UCB Lyon 1), 69100 Villeurbanne, France

<sup>‡</sup>Department of Chemistry, Laboratory of Inorganic Chemistry, ETH Zürich, CH-8093, Zürich, Switzerland

## Supporting Information

**ABSTRACT:** Dynamic nuclear polarization (DNP) solid-state NMR has been applied to powdered microcrystalline solids to obtain sensitivity enhancements on the order of 100. Glucose, sulfathiazole, and paracetamol were impregnated with bis-nitroxide biradical (bis-cyclohexyl-TEMPO-bisketal, bCTbK) solutions of organic solvents. The organic solvents were carefully chosen to be nonsolvents for the compounds, so that DNP-enhanced solid-state NMR spectra of the unaltered solids could be acquired. A theoretical model is presented that illustrates that for externally doped organic solids characterized by long spin–lattice relaxation times ( $T_1(^1\text{H}) > 200$  s),  $^1\text{H}$ – $^1\text{H}$  spin diffusion can relay enhanced polarization over micrometer length scales yielding substantial DNP enhancements ( $\epsilon$ ).  $\epsilon$  on the order of 60 are obtained for microcrystalline glucose and sulfathiazole at 9.4 T and with temperatures of ca. 105 K. The large gain in sensitivity enables the rapid acquisition of  $^{13}\text{C}$ – $^{13}\text{C}$  correlation spectra at natural isotopic abundance. It is anticipated that this will be a general method for enhancing the sensitivity of solid-state NMR experiments of organic solids.



## INTRODUCTION

Solid-state NMR is the richest source of structural and dynamic information for powdered solids. Today it is probably most widely employed to characterize powdered (microcrystalline) molecular samples, and experiments employing  $^1\text{H}$ ,  $^{13}\text{C}$ , and increasingly other nuclei (e.g.,  $^{15}\text{N}$ ,  $^{19}\text{F}$ ,  $^{31}\text{P}$ ,  $^{35}\text{Cl}$ , etc.) are now routinely employed as probes of structure and packing (i.e., hydrogen bonding).<sup>1–15</sup> For example, structural polymorphism is an issue of great importance for pharmaceutically relevant compounds, and solid-state NMR is today a primary tool for investigating and differentiating polymorphs.<sup>4,7,16–21</sup> In favorable cases it is possible to determine complete de novo three-dimensional crystal structures from solid-state NMR of powders. Such NMR crystallography approaches are performed with a number of techniques, using NMR alone, or in combination with DFT chemical shift calculations, structure prediction methods, or powder X-ray diffraction.<sup>22–30</sup>

However, the main limitation to the broader application of these methods is the poor sensitivity of NMR. This can be illustrated through the low sensitivity of natural abundance  $^{13}\text{C}$  or  $^{15}\text{N}$  experiments. It is often impractical to record  $^{15}\text{N}$  spectra at natural abundance except for the simplest, most concentrated compounds. *Even in favorable cases*, two-dimensional  $^{13}\text{C}$ – $^{13}\text{C}$  correlation experiments or one-dimensional spectral editing experiments require times on the order of days. Such experiments are usually unavoidable to assign resonances, with the assignment step being essential to determine detailed structures or dynamics. For compounds with unfavorable

properties (e.g.,  $Z' > 1$ , many inequivalent resonances, disorder, or unfavorable nuclear relaxation properties) one-dimensional spectra are often a challenge and it is usually impossible to perform more complex NMR experiments.

Long relaxation times are particularly problematic. Rigid compounds, for example, sulfathiazole,<sup>31</sup> glucose (vide infra), and many other organic solids,<sup>32–37</sup> typically possess proton spin–lattice relaxation times ( $T_1(^1\text{H})$ ) ranging from 150 to 1000 s at room temperature. In comparison, compounds, such as most proteins, which are flexible and/or possess methyl groups, are characterized by short  $T_1(^1\text{H})$  on the order of  $\sim 2$  s. The sensitivity of solid-state NMR experiments will thus be reduced by at least an order of magnitude in such compounds.<sup>38</sup> One solution to the relaxation time problem is to add low concentrations of paramagnetic impurities into the crystalline lattice to enhance relaxation;<sup>32,33,39</sup> however, this cannot be a general approach as doping requires recrystallization or irradiation and results in modified or impure phases. In particular, for example, it is not applicable to the study of polymorphs.

One intriguing possibility to enhance sensitivity of solid-state NMR of powdered microcrystalline samples would be to apply dynamic nuclear polarization (DNP). Although DNP was first proposed and demonstrated in the 1950s,<sup>40–42</sup> high-field DNP solid-state NMR experiments have only very recently become

Received: August 16, 2012

Published: September 11, 2012

feasible with the introduction of high power, THz frequency gyrotron microwave sources and cryogenic magic angle spinning (MAS) probes by the Griffin research group.<sup>43–46</sup> In such experiments the polarization of unpaired electrons is transferred to nuclei, providing a maximum signal enhancement from an electron equal to  $\gamma_e/\gamma_X$  ( $\sim 658$  for  $^1\text{H}$ ), where  $\gamma_e$  and  $\gamma_X$  are the gyromagnetic ratios of the electron and polarized nucleus, respectively. At 9.4 T with biradical polarizing agents<sup>47–52</sup> and sample temperatures of  $\sim 100$  K proton DNP enhancements ( $\epsilon_{\text{H}}$ ) greater than 20 (and up to 105,<sup>50</sup> or up to 230 at 5 T and 82 K)<sup>52</sup> and sensitivity enhancements of 2 orders of magnitude are routinely obtained.<sup>50,53</sup> This has led to the immediate application of DNP to enhance the sensitivity of solid-state NMR experiments on a variety of biological<sup>54–63</sup> and materials systems.<sup>50,64–69</sup>

Interestingly, in almost all examples the source of polarization, usually an exogenous stable biradical,<sup>47–52</sup> is intimately mixed with the sample. This is accomplished either by dissolving or suspending the material in the radical solution, which is then frozen during the course of experiments.<sup>45</sup> Surfaces of materials may be polarized by impregnating the sample with a radical-containing solution.<sup>64</sup> This places the radical in close proximity to the surface, providing a high  $\epsilon$ . Materials such as diamond have also been polarized by using intrinsic lattice defects.<sup>70–72</sup> In a departure from these experiments, van der Wel et al. showed that a nanocrystalline polypeptide (with 50–200 nm crystal widths) suspended in a frozen radical-containing solution could be efficiently polarized even if the radicals were restricted to the crystal surfaces.<sup>54</sup> This study clearly demonstrated that enhanced polarization could diffuse from the surface of the crystals into their interiors by  $^1\text{H}$ – $^1\text{H}$  spin diffusion so that the whole crystals could be polarized.

While many of these systems are clearly of very high interest in modern chemistry and biology, and these experiments have attracted great attention, so far DNP has not been shown for ordinary microcrystalline solid-state NMR. Here we show how DNP-enhanced NMR spectra can be obtained from microcrystalline solids by impregnation with radical-containing organic solutions, where the impregnating liquids are carefully chosen to be nonsolvents for the compounds. We show how for such externally doped organic solids  $^1\text{H}$ – $^1\text{H}$  spin diffusion can relay enhanced polarization over micrometer length scales, yielding substantial bulk DNP enhancements ( $\epsilon$ ). In this way we acquire DNP-enhanced solid-state NMR spectra of powdered samples of glucose and sulfathiazole, which serve as examples of small molecules that are characterized by a long  $T_1(^1\text{H})$ . With this procedure  $\epsilon > 50$  and sensitivity enhancements ( $\Sigma^\dagger$ )  $> 150$  can be obtained in comparison to standard room temperature solid-state NMR experiments for compounds possessing a long  $T_1(^1\text{H})$ . The theoretical framework of Griffin and co-workers<sup>54</sup> that describes the influence of  $T_1(^1\text{H})$  and crystal size on  $\epsilon_{\text{H}}$  is modified to account for the spherical symmetry of particulate crystalline solids and a distribution of particle sizes. The theoretical signal build-up curves and the variation in  $\epsilon_{\text{H}}$  as a function of the recycle delay for typical microcrystalline solids are compared to experimental results and the agreement is found to be excellent. Additionally, for compounds with long  $T_1(^1\text{H})$ , the optimal repetition delay is decreased due to spin diffusion from the fast relaxing surface coating, and is found to be much shorter than  $T_1(^1\text{H})$ . Overall gains in sensitivity  $\Sigma^\dagger$  are thus found to be of the order of 150. This enables the acquisition of natural abundance  $^{13}\text{C}$ – $^{13}\text{C}$

through-bond (refocused INADEQUATE)<sup>73</sup> and dipolar (POST-C7)<sup>74</sup> correlation spectra in less than 18 h. Experiments were also performed on paracetamol, a compound characterized by a short  $T_1(^1\text{H})$  and a more modest  $\epsilon$  and  $\Sigma^\dagger$  of  $\sim 5$  was obtained.

## EXPERIMENTAL SECTION

Samples of anhydrous  $\alpha$ -D-glucose (glucose), 4-amino-*N*-(2-thiazolyl)-benzenesulfonamide (sulfathiazole), and *N*-acetyl-4-aminophenol (paracetamol) were obtained from Sigma Aldrich and used without further purification. Prior to preparation of samples for DNP experiments the samples were finely ground by hand in a mortar and pestle for several minutes, unless noted otherwise. The glucose samples were characterized by scanning electron microscopy (FEI Quanta 200 FEG ESEM). In a typical preparation, 10–20  $\mu\text{L}$  of 16 mM bis-nitroxide biradical (here bis-cyclohexyl-TEMPO-bisketal, bCTbK) solution was added to ca. 40 mg of powdered solid. The wet powder was then mixed with a glass stirring rod and transferred to a sapphire rotor and capped with a polyfluoroethylene insert. The weight of the dry powder, the impregnated powder, and the empty and the filled rotor were all recorded so that the composition and amount of material in each rotor could be determined (Table S1, SI). The organic solvents utilized for DNP experiments<sup>66</sup> were visually screened to determine if the microcrystalline solids were insoluble. Solution NMR experiments were then used to confirm the insolubility of the solids in a given solvent (Figure S1, SI). bCTbK was used as a polarization source since it reliably provides an  $\epsilon_{\text{H}}$  of ca. 100 when combined with halogenated solvents.<sup>50</sup>

All solid-state NMR experiments were performed on a 9.4 T Bruker Avance III solid-state NMR spectrometer that was equipped with a 3.2 mm double-resonance low-temperature MAS probe and a Bruker Biospin low-temperature cooling cabinet.<sup>75</sup> For DNP experiments the samples were cooled to ca. 105 K. The sweep coil of the main magnetic field ( $\nu_0(^1\text{H}) = 400.432$  MHz) was set so that microwave irradiation occurred at the same position as the  $\epsilon$  maximum for TOTAPOL.<sup>48</sup> The estimated power of the microwave beam at the output of the waveguide was 4 W. The sample spinning rate ( $\nu_{\text{rot}}$ ) was 8000 Hz in all cases. For all CP experiments the amplitude of the  $^1\text{H}$  rf field was ramped during the contact time to improve efficiency.<sup>76</sup> SPINAL64 decoupling was applied during acquisition and echo delays in refocused INADEQUATE experiments.<sup>77</sup> Additional details on solid-state NMR experiments can be found in Table S2 (SI).  $\epsilon$  was measured by comparing the intensity of the spectra acquired with and without microwave irradiation. Numerical spin diffusion models were constructed with MatLab v7.10 (The MathWorks, Inc.).

## RESULTS AND DISCUSSION

**Theoretical Models for Understanding the Effect of Crystal Size and  $T_1(^1\text{H})$  on  $\epsilon_{\text{H}}$ .** The theoretical model is similar to that presented by Griffin and co-workers;<sup>54</sup> however, here we develop a framework suited to samples with long  $T_1$  values and larger three-dimensional objects. Notably the framework is numerical and is not limited to the steady state. We note in passing that several other research groups have presented models describing the enhanced longitudinal relaxation of systems heterogeneously doped with paramagnets.<sup>39,78–80</sup>

**Diffusion Equation.** The aim is to simulate polarization build-up curves for crystalline materials externally coated with radical solutions. The model must account for experiments with and without microwave irradiation to drive DNP. The starting point here for the analysis is the diffusion/transport equation under the assumption that the crystals possess spherical symmetry:

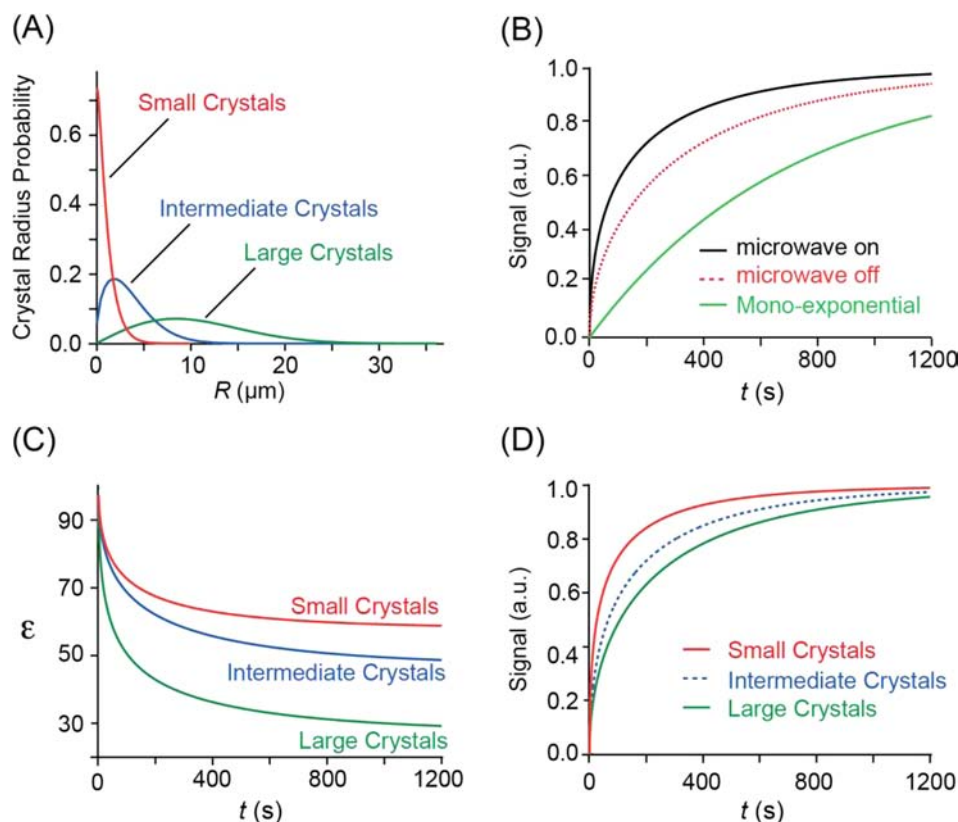


**Figure 1.** Calculated signal build-up rates and  $\epsilon$  as a function of time. For B to E the  $T_{1,\text{core}}$  was assumed to be 700 s and the  $T_{1,\text{surf}}$  was 1 ms. (A) Three crystal radius (Weibull) distributions used for the calculations. (B) The calculated signal as a function of build-up time for an intermediate crystal distribution. The signal build-ups calculated for experiments with and without microwave irradiation are shown. A monoexponential signal build-up for a 700 s  $T_1$  is also shown for comparison. (C) The calculated  $\epsilon$  as a function of time for the three crystal size distributions. (D) Signal build-up curves for the three crystal size distributions. The signal build-ups in parts B and D are all normalized to 1 at infinite time.

$$\frac{\partial P(r, t)}{\partial t} = D \left( \frac{\partial^2 P(r, t)}{\partial r^2} + \frac{2}{r} \frac{\partial P(r, t)}{\partial r} \right) - \frac{P(r, t) - P_0(r)}{T_1(r)} \quad (1)$$

where  $r$  is the distance from the center of the spherical crystal in angstroms ( $0 < r < \text{crystal radius}, R$ ),  $t$  is time in seconds ( $0 < t < \infty$ ),  $P$  represents polarization, which is a function of position ( $r$ ) and time ( $P(r, t)$ ), and  $P_0(r)$  is the local equilibrium polarization in the absence of spin diffusion (for example, thermal equilibrium corresponds to  $P_0(r) = 1$ ). To solve eq 1 we make the following assumptions: (i) we assume that at the surface of the crystal there is a layer for which  $T_1$  is reduced by direct paramagnetic relaxation. The  $T_1$  at the surface is short ( $T_{1,\text{surf}}$  taken here to be 1 ms). The  $T_1$  of the nuclei near the surface increases with increasing distance from the surface with a classical ( $r^{-6}$ ) dependence. Within a few tens of angstroms from the surface  $T_1$  attains the value of the intrinsic core  $T_1$  ( $T_{1,\text{core}}$  assumed here to be 700 s, see Figure S2 in the SI for more details). (ii)  $P_0(r)$  is set as follows: for the case of no microwave irradiation, the equilibrium polarization is chosen to be 1 everywhere. For simulations with microwave irradiation to drive DNP, we consider that a 20 Å shell is directly enhanced by DNP. For this shell  $P_0$  is 100, while for the rest of the crystal  $P_0$  is 1. Under the influence of eq 1, spin diffusion will then tend to equalize polarization throughout the crystal.

Here we do not assume a steady state condition, since  $T_{1,\text{core}}$  for the microcrystalline samples is often greater than 500 s at

low temperatures, and a steady state is not usually achieved in the experiments. The initial and boundary conditions are respectively:

$$P(r, 0) = 0 \quad (2)$$

$$D \frac{\partial P(R, t)}{\partial r} - \frac{R}{T_{1,\text{surf}}} [P(R, t) - P_0(R)] = 0 \quad (3)$$

where  $R$  corresponds to the position at the surface (the crystal radius). The initial condition 2 corresponds to a saturated state, while condition 3 is a Neumann boundary condition,<sup>80,81</sup> which corresponds to no polarization diffusing out of the crystal (i.e., there can only be diffusion of polarization from the surface of the crystal inward; this is physically reasonable if the radical-containing solvent layer has a short  $T_1$ , which will always be the case here). With these two conditions eq 1 can be numerically integrated to obtain the polarization as a function of time and position. If the polarization is integrated over the spherical crystal, the volume weighted signal build-up function  $[S(t, R)]$  for a crystal of radius  $R$  can be obtained:

$$S_{\text{on/off}}(t, R) = \int_0^R P_{\text{on/off}}(r, t) r^2 dr \quad (4)$$

where  $S_{\text{on}}$  corresponds to the microwave irradiation case and  $S_{\text{off}}$  corresponds to no microwaves. The DNP enhancement for a single crystallite as a function of time can then be calculated as:

$$\varepsilon(t, R) = \frac{S_{\text{on}}(t, R)}{S_{\text{off}}(t, R)} \quad (5)$$

**Modeling Crystal Size Distributions.** In general a microcrystalline sample will be inhomogeneous and possess a distribution of crystal sizes (see, for example, the SEM images below). For this reason the signals from different crystals are averaged over a distribution of crystal sizes:

$$\overline{S_{\text{on/off}}(t)} = \frac{\sum_{\text{crystallites}} S_{\text{on/off}}(t, R)g(R)}{\sum_{\text{crystallites}} g(R)} \quad (6)$$

where  $g(R)$  is the probability of finding a crystal of radius  $R$  in the sample. Here we use  $g(R)$  in the form of a Weibull distribution (Figure 1A, eq S1 in the SI) to mimic distributions of crystal sizes encountered in real samples.<sup>82,83</sup> Typically the crystal size averaging in the following is conducted by summing over 50 different crystal sizes.

For a given distribution of crystal sizes the average DNP enhancement is:

$$\overline{\varepsilon(t)} = \frac{\sum_{\text{crystallites}} \varepsilon(t, R)g(R)R^3}{\sum_{\text{crystallites}} g(R)R^3} \quad (7)$$

The  $R^3$  term is necessary to weigh the DNP enhancements by the volume of the individual crystallites.

**Predicted Enhancements for Microcrystalline Samples.** Calculated signal build-up curves and the variation in  $\varepsilon$  as a function of time obtained from the model developed above are shown in Figure 1.

Figure 1B shows the calculated signal intensity as a function of recycle delay for the intermediate crystal size distribution. It shows the signal build-up for microwave on and microwave off signals, normalized to the same equilibrium (final) values. This highlights that the two build-ups will have different dynamics, since in one case the equilibrium polarization at the surface ( $P_0$ ) is a factor 100 times larger. Both curves are multi-exponential, due both to the relaxation sink present at the surface and to the crystal size distribution. These features are all confirmed experimentally below. This is contrasted in Figure 1B with the behavior of a dry powder, which would be monoexponential with a build-up rate constant of  $T_{1,\text{core}}$ .

In parts C and D of Figure 1 we show how the difference in signal build-up rates gives rise to a variation in  $\varepsilon$  as a function of the recycle delay employed (Figure 1C). Note that this would not be noticed in steady-state DNP experiments, as is the case for most dispersed samples with short  $T_1$ , but is in fact predicted to be a large effect here, with much higher  $\varepsilon$  predicted for shorter recycle times. Figure 1C also shows how  $\varepsilon$  varies with crystal size: smaller sizes produce larger  $\varepsilon$  and faster build-ups. Another interesting feature of the model is that it predicts that  $\varepsilon$  at the center of the crystals is substantial (Figure S3, SI), which illustrates the large length scales over which polarization can diffuse. Finally, we stress that the enhanced signal build-up rate for nuclei in the crystal does not arise primarily from direct paramagnetic relaxation, but rather from polarization diffusion relayed from the fast relaxing/highly polarized nuclei at the surface of the crystal.

With the theoretical model the influence of core  $T_1$  values on  $\varepsilon$  can also be calculated (Figure 2). As expected, with larger values of the core  $T_1$  values the DNP enhancements are larger since enhanced polarization can diffuse over greater distances before being dispersed by longitudinal relaxation. However,

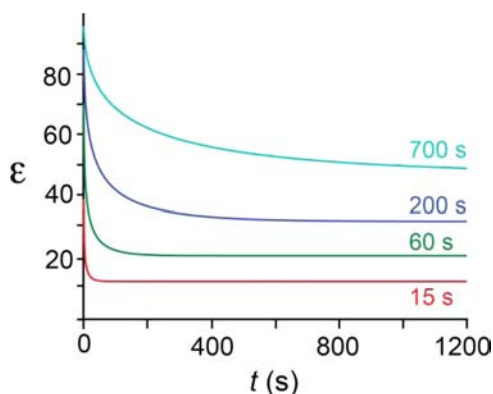


**Figure 2.** The calculated values of  $\varepsilon$  as a function of  $t$  for  $T_{1,\text{core}}$  values of 700, 200, 60, and 15 s.

longer core  $T_1$  values are also predicted to be accompanied by slower signal build-up rates (Figure S3, SI). We note that for a  $T_1(^1\text{H})$  of 15 s, a substantial  $\varepsilon$  on the order 10 is still expected. This is consistent with the  $\varepsilon$  experimentally observed for paracetamol (vide infra).

**DNP Solid-State NMR Experiments on Microcrystalline Glucose.** Glucose was chosen for this study because it possesses a long  $T_1(^1\text{H})$  of ca. 180 s at room temperature. The  $T_1$  at 100 K is ca. 650 s. Prior to DNP experiments, its solubility in several organic liquids suitable for DNP<sup>66</sup> was screened by visual inspection and solution NMR experiments (Table S2 and Figure S1, SI). Glucose was found to be insoluble or very weakly soluble in several organic liquids. 1,1,2,2-Tetrabromoethane ( $\text{EtBr}_4$ ) was chosen since the  $^{13}\text{C}$  chemical shift of this solvent (centered around 47 ppm) has minimal overlap with the glucose resonances. The bCTbK biradical was employed as a polarizing agent because it reliably provides an  $\varepsilon_{\text{H}}$  of ca. 100 when combined with halogenated solvents. The glucose sample was finely ground by hand in a mortar and pestle to reduce the average grain size. The sample was impregnated with a minimal amount of 16 mM bCTbK  $\text{EtBr}_4$  solution by using the incipient wetness impregnation technique,<sup>64</sup> then transferred to a sapphire rotor.

DNP-enhanced CP/MAS  $^{13}\text{C}$  solid-state NMR spectra of impregnated glucose acquired with a saturation recovery  $^1\text{H}$ - $^{13}\text{C}$  CP pulse sequence (Figure 3A) are shown in Figure 3B.  $^{13}\text{C}$  DNP enhancements obtained with cross-polarization ( $\varepsilon_{\text{C CP}}$ ) greater than 60 are readily obtained, and as predicted above the magnitude of  $\varepsilon_{\text{C CP}}$  depends upon the recycle delay ( $\tau$ ) used to acquire the spectra (Figure 3C). With DNP very high signal-to-noise ratio (S/N) spectra can be rapidly acquired. For example, for the spectrum acquired with microwave irradiation and a 60 s recycle delay the S/N is ca. 750 after only 4 scans.

Importantly, we note that despite the fact that the samples are cooled to 100 K to obtain a large  $\varepsilon$ , the resolution of the spectrum is comparable to that obtained at room temperature, with average full widths at half height ( $\Lambda$ ) of 0.33 ppm at 105 K as compared to 0.28 ppm at 298 K for dry powdered glucose (Figure S4 and Table S4, SI). The high spectral resolution observed here contrasts with that typically observed in DNP solid-state NMR experiments on molecules dissolved/immobilized in glass-forming solvents where  $\Lambda$  is typically on the order of 2–5 ppm.<sup>68,84</sup> The small  $\Lambda$  for glucose (and other microcrystalline solids, vide infra) at 105 K are obtained because such rigid molecules exist in a highly ordered

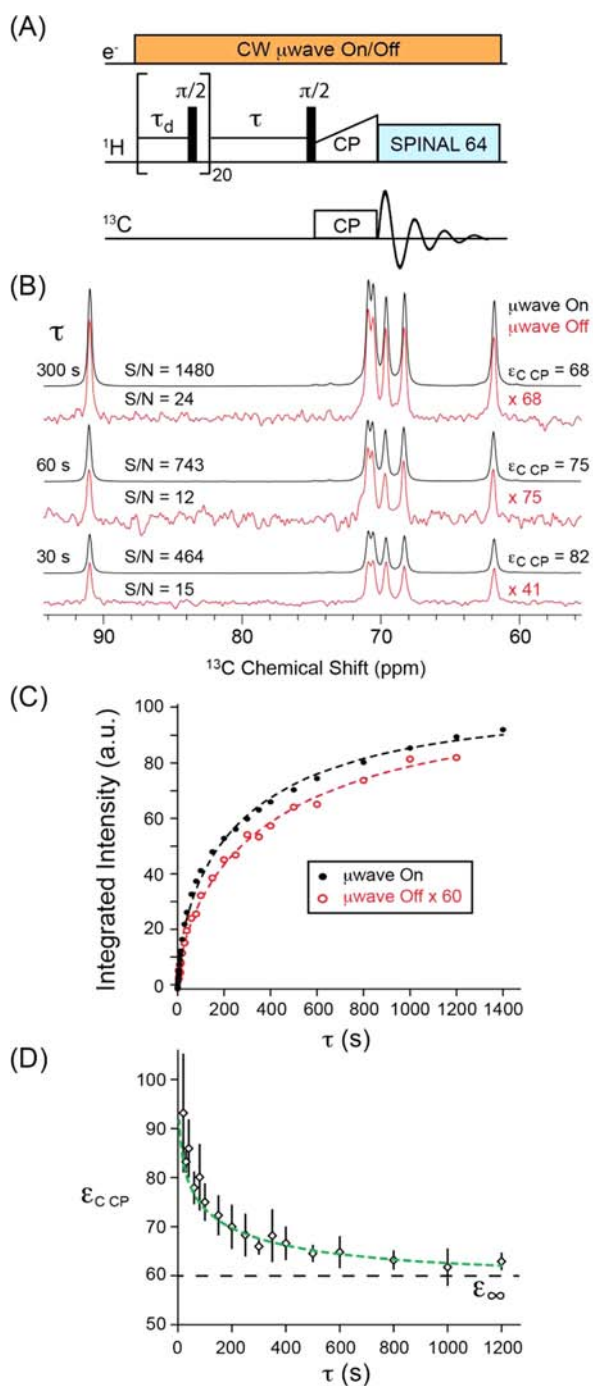


**Figure 3.** (A) The saturation recovery  $^1\text{H}$ - $^{13}\text{C}$  CP pulse sequence used for acquisition of spectra.  $\tau_d$  was set to 4 ms. (B)  $^1\text{H}$ - $^{13}\text{C}$  CP/MAS solid-state NMR spectra of glucose impregnated with 16 mM bCTbK EtBr<sub>4</sub> solution. The recycle delay ( $\tau$ ),  $\epsilon_{\text{CP}}$ , intensity scaling factor of the microwave off spectrum and S/N ratio of each spectrum are provided. All spectra acquired with a sample spinning rate ( $\nu_{\text{rot}}$ ) of 8000 Hz. Four scans were acquired except for the microwave off 30 s recycle delay spectrum for which 8 scans were acquired. (C) Normalized signal intensities as a function of  $\tau$  for the  $^{13}\text{C}$  resonance at 90.7 ppm acquired with (black) and without (red) microwave irradiation. Stretched exponential fits of the experimental curves are shown in dashed lines. The results of the curve fitting are given in Table 1. (D) The measured value of  $\epsilon_{\text{CP}}$  as a function of  $\tau$  (open circles) and values calculated with a ratio of stretched exponential functions (green line).

environment within the crystalline lattice that does not become disordered at low temperature. This is consistent with Griffin and co-workers who obtained high resolution for microcrystalline tripeptides at 85 K.<sup>85</sup>

**Relaxation Measurements and Quantification of DNP Sensitivity Enhancements.** To properly assess the gain in sensitivity provided by 105 K DNP experiments as compared to standard room temperature solid-state NMR experiments on dry solids it is necessary to measure  $T_1(^1\text{H})$ . Indeed cooling the sample to 105 K will significantly increase relaxation times, while the presence of radicals at the surface of the crystal should partially offset this by spin diffusion relayed enhanced relaxation, as discussed above. Figure 3C shows the integrated intensity of the  $^{13}\text{C}$  resonance at 90.7 ppm as a function of  $\tau$  at 105 K for microwave on and off experiments (normalized to the same maximum, the microwave off integrals are actually a factor 60 more intense). The resulting curves can be fit with a stretched exponential function of the form:

$$S(\tau) = A \left[ 1 - \exp\left(-\left(\frac{\tau}{T_1^*}\right)^\beta\right) \right] \quad (8)$$

where  $S$  is the signal (integral) intensity,  $\tau$  is the recycle delay in s,  $A$  is the equilibrium signal intensity in arbitrary units,  $\beta$  is a unit-less scalar, and  $T_1^*$  is the observed signal build-up time constant. Stretched exponential functions are typically used to model the build up of magnetization in organic solids heterogeneously doped with paramagnets.<sup>79,80,86</sup> The signal build-up time constant has been denoted  $T_1^*$  to differentiate it from  $T_1(^1\text{H})$ .  $T_1(^1\text{H})$  is not measured here since the signal build-up is driven by the diffusion of polarization from fast relaxing/highly polarized surface nuclei in addition to longitudinal relaxation. The measurements for each of the resolved  $^{13}\text{C}$  resonances are summarized in Table 1.

**Table 1. Summary of Relaxation Measurements on Glucose Impregnated with a 16 mM bCTbK EtBr<sub>4</sub> Solution<sup>a</sup>**

resonance	90.7 ppm	68.0 ppm	61.5 ppm	av values
with microwave				
$A_{\text{on}}$ (au)	97(3)	95(3)	86(3)	
$T_1^*$ (s)	309(34)	293(33)	277(28)	293(16)
$B$	0.60(2)	0.60(2)	0.60(2)	0.60
without microwave				
$A_{\text{off}}$ (au)	1.6(1)	1.6(1)	1.4(1)	
$T_1^*$ (s)	440(72)	330(43)	399(60)	390(55)
$B$	0.64(3)	0.70(3)	0.66(3)	0.66(3)
$\epsilon_{\infty}$	61(4)	60(3)	60(3)	60(1)

<sup>a</sup>The relaxation data were fit with a stretched exponential function of the form  $S(\tau) = A[1 - \exp(-(\tau/T_1^*)^\beta)]$ . <sup>b</sup>Uncertainties associated with the fit are given in parentheses (e.g., 309(34) s = 309 ± 34 s). For the average values the uncertainties correspond to the standard deviation. <sup>c</sup> $\epsilon_{\infty}$  is the DNP enhancement that would be measured for long recycle delays ( $\tau > 10T_1$ ),  $\epsilon_{\infty} = (A_{\text{on}})/(A_{\text{off}})$ .

Measurements with DNP reveal that the average value of  $T_1^*$  is 293 s and the average  $\beta$  exponential is 0.60. The deviation of  $\beta$  from 1 (the monoexponential case) is consistent with the existence of a continuum of apparent longitudinal recovery rates, which is consistent with the theoretical model. For experiments without microwave irradiation the average  $T_1^*$  was found to be 390 s and  $\beta$  was found to be slightly increased to 0.66. The difference in the value of  $T_1^*$  for DNP and standard

experiments is predicted by the model (*vide supra*). Indeed, comparison of the predicted behavior of Figure 1B and the experiment in Figure 3C shows very good agreement. Finally, the experimentally observed variation in  $\epsilon_{\text{CP}}$  is shown in Figure 3D and once again clearly reproduces the predictions of Figure 1C extremely well. The steady state value of the DNP enhancement ( $\epsilon_{\infty}$ ) is estimated to be 60.

The overall sensitivity enhancement ( $\Sigma$ ) available from the 105 K DNP experiments as compared to room temperature experiments on dry powders can be estimated as follows. Given the low surface area of the microcrystalline samples we assume that signal attenuation by paramagnetic relaxation effects (“quenching” or “bleaching”)<sup>53,87,88</sup> can be neglected. If the noise level is taken to be the same for experiments at 105 and 298 K the sensitivity enhancement can be estimated as:

$$\Sigma^{\dagger} = [\epsilon(\tau_1)] \left( \frac{\Lambda_{298\text{K}}}{\Lambda_{\text{DNP}}} \right) \left( \frac{298\text{ K}}{105\text{ K}} \right) \frac{S_{\text{on}}(\tau_1)}{S_{298\text{K}}} \sqrt{\frac{\tau_2}{\tau_1}}$$

$$\Sigma^{\dagger} = [\epsilon(\tau_1)] \left( \frac{\Lambda_{298\text{K}}}{\Lambda_{\text{DNP}}} \right) \left( \frac{298\text{ K}}{105\text{ K}} \right) \left( \frac{1 - \exp(-(\tau_1/T_1^*)^\beta)}{1 - \exp(-(\tau_2/T_{1,289\text{K}}))} \right) \sqrt{\frac{\tau_2}{\tau_1}} \quad (9)$$

where  $\Lambda_{105\text{K}}$  and  $\Lambda_{298\text{K}}$  are the average full widths at half height of the carbon resonances at 105 and 298 K,  $T_{1,298\text{K}}$  is the  $T_1(^1\text{H})$  for glucose at room temperature,  $\tau_1$  and  $\tau_2$  are the recycle delays that provide optimal signal-to-noise per unit time for each temperature, and  $\epsilon(\tau_1)$  is the DNP enhancement for recycle delay  $\tau_1$ . In both cases the signal functions ( $S(\tau)$ ) have been normalized to 1. The  $\Lambda$  ratio in this case is 0.85 and this term accounts for signal loss by broadening of the resonances at lower sample temperatures. The ratio of temperatures accounts for additional signal enhancement from thermal Boltzmann enhancement, while the ratio of  $\tau_2$  and  $\tau_1$  determines the gain (or loss) in repetition rate for signal averaging. It should be noted that eq 9 does not account for any potential gains in CP efficiency that are also usually realized at low temperatures.

For dry powdered glucose at room temperature the signal build-up is characterized by a monoexponential function with  $T_1(^1\text{H}) = 180$  s. Therefore, the optimal recycle delay for room temperature experiments is  $\tau_2 = 1.3 \times 180$  s = 234 s. A measurement of the normalized value of  $[S_{\text{on}}/(\tau)^{1/2}]$  for the DNP-enhanced solid-state NMR spectra as a function of  $\tau$  was made to determine the value of  $\tau_1$  (Figure S5, SI). Optimal S/N for the DNP experiments on glucose is obtained with  $\tau = 60$  s. With a recycle delay of 60 s  $\epsilon_{\text{CP}}$  was 75. Therefore, with eq 9 the gain in sensitivity provided by the DNP experiments is calculated to be  $\sim 150$ , in comparison to room temperature experiments on dry powders conducted with the same spectrometer.

**Acquisition of Natural Abundance 2D  $^{13}\text{C}$ – $^{13}\text{C}$  Correlation Spectra.** For glucose the large sensitivity enhancements provided by low-temperature DNP experiments enable the acquisition of  $^{13}\text{C}$  CP/MAS spectra with S/N of ca. 1000 in experiment times on the order of minutes. It is necessary to have a high level of S/N for natural abundance  $^{13}\text{C}$ – $^{13}\text{C}$  correlation experiments since the S/N will be reduced by at least a factor of 100 by the double-quantum  $^{13}\text{C}$  filter. Figure 4 shows a 2D  $^{13}\text{C}$ – $^{13}\text{C}$  through-bond refocused INADEQUATE<sup>73</sup> spectrum. The INADEQUATE spectrum enables the connectivity of the molecule to be determined,

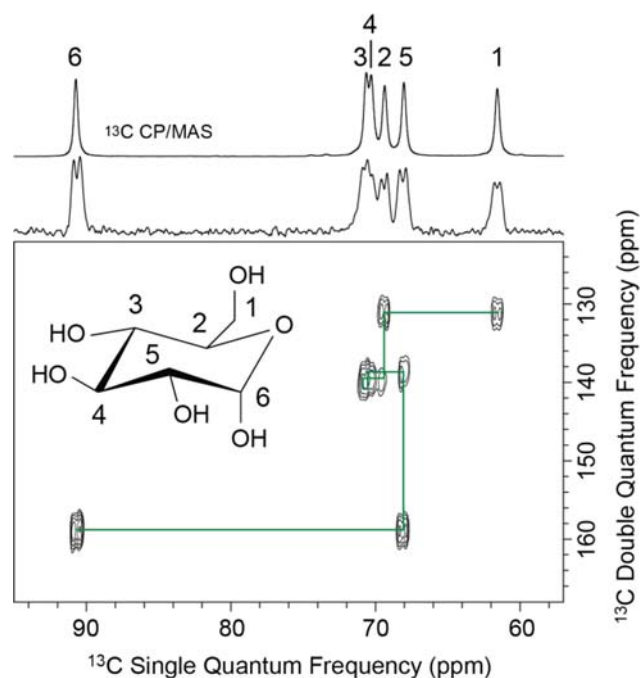


**Figure 4.** 2D refocused INADEQUATE  $^{13}\text{C}$ – $^{13}\text{C}$  correlation spectrum of glucose acquired at natural isotopic abundance. A  $^{13}\text{C}$  CP/MAS spectrum acquired with 4 scans and a 60 s recycle delay is overlaid on top of the projection spectrum for comparison. The spectrum was acquired in a total experiment time of 16 h (30 s recycle delay, 30  $t_1$  increments, 64 scans per  $t_1$  increment, and  $\Delta t_1 = 100$   $\mu\text{s}$ ). A 4 ms delay was employed for generation of double quantum coherences. The molecular structure of glucose is shown and the carbon resonances are assigned. The connectivity of the carbon atoms is mapped out on the 2D spectrum (green line). Note that the one bond carbon–carbon scalar ( $J$ ) couplings are resolved in  $\omega_2$  dimension of the INADEQUATE spectrum.

which immediately yields the assignment of the complete carbon-13 spectrum. We note that the carbon–carbon  $J$ -couplings are well resolved in  $\omega_2$ , highlighting the high resolution of the low-temperature spectrum. A natural abundance through-space (dipolar) 2D POST-C7<sup>74,89</sup>  $^{13}\text{C}$ – $^{13}\text{C}$  correlation spectrum was also acquired (Figure S6, SI). The dipolar correlation POST-C7 spectrum probes through-space contacts. We note that both 2D spectra were acquired with experiment times of only ca. 16 h each (see the SI). For comparison, the acquisition of natural abundance  $^{13}\text{C}$  2D INADEQUATE spectra of microcrystalline organic complexes with favorable relaxation characteristics usually requires experiment times on the order of 3 to 10 days even with larger size rotors and higher static magnetic fields than those used here.<sup>90–92</sup> Acquisition of a  $^{13}\text{C}$ – $^{13}\text{C}$  correlation spectrum of crystalline glucose without DNP would require months of spectrometer time. This clearly demonstrates the large sensitivity enhancement provided by DNP.

**The Influence of Grain Size on  $\epsilon$  and  $\Sigma^{\dagger}$ .** The effects of the grain size on  $\epsilon$  and  $\Sigma$  were investigated by performing DNP experiments on both glucose ground by hand in a mortar and pestle and on as-received glucose (Figure 5). Scanning electron microscope (SEM) images of both samples are also pictured (Figure 5, and in the SI Figure S8).<sup>93</sup>

As predicted in the theory section, for the ground and as-received samples we observed  $\epsilon_{\text{CP}}$  of 60 and 35, respectively, for experiments conducted with a  $\tau$  of 10 s. In addition to the

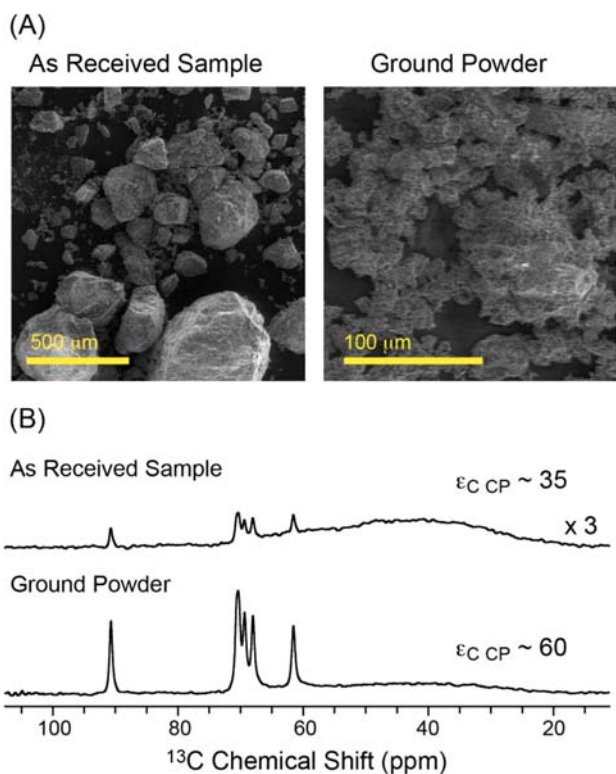


**Figure 5.** (A) SEM images (FEI Quanta 200 FEG ESEM) of the as-received microcrystalline glucose and glucose that was ground by hand in a mortar and pestle. (B) DNP-enhanced  $^1\text{H}$ - $^{13}\text{C}$  CP/MAS spectra of the as-received glucose and ground glucose acquired with 4 scans and a 10 s recycle delay.  $\epsilon_{\text{CP}}$  is nearly double for the ground powder and the signal is ca. 11.5 times greater, likely due to more favorable relaxation properties. The broad resonance of  $\text{EtBr}_4$  centered around 45 ppm is also visible.

reduction in  $\epsilon_{\text{CP}}$  for the as-received sample, the signal per unit mass of the as-received sample was 11.5 times lower than that of the ground sample, reflecting a large reduction in  $\Sigma^{\dagger}$ . This reduction in  $\Sigma^{\dagger}$  occurs because both the  $\epsilon_{\text{CP}}$  and the relaxation properties of the as-received sample will be less favorable due to the lower accessible surface area, and larger grain size. SEM images of the two samples show that the grain sizes are heterogeneous in both samples; however, for the as-received sample there are many more large particles, with particles as large as 500 μm present (Figure 5). Conversely, in the ground sample there are many more sub-20 μm diameter grains. Both the reduction in  $\epsilon$  and an increase in  $T_1^*$  are predicted for larger grain sizes by our theoretical model (vide supra). This illustrates that by simply grinding the sample by hand prior to DNP experiments, larger enhancements and improved sensitivity can be obtained. (Although we note that this may not always be possible since some polymorphs are sensitive to even gentle grinding. In rare cases, extreme grinding may also introduce defects into the crystal or at the surface that enhance longitudinal relaxation rates;<sup>80,86,94</sup> which might reduce the DNP enhancement that could be obtained.)

**DNP-Enhanced Solid-State NMR Spectra of Microcrystalline Sulfathiazole.** Sulfathiazole is a classic system that displays polymorphism and has been extensively studied.<sup>31</sup> Sulfathiazole lacks methyl groups and  $T_1(^1\text{H})$  for sulfathiazole is between 200 and 500 s at 298 K for the various polymorphs.<sup>31</sup> Experiments were performed on a sample of ground sulfathiazole impregnated with a 16 mM bCTbK 1,3-

dibromobutane ( $\text{BuBr}_2$ ) solution.  $\text{BuBr}_2$  provides lower DNP enhancements than  $\text{EtBr}_4$ ; however, this liquid was necessary because sulfathiazole is soluble in  $\text{EtBr}_4$ .

The  $^1\text{H}$ - $^{13}\text{C}$  CP/MAS spectra of sulfathiazole acquired with and without microwave irradiation are shown in Figure 6A. All

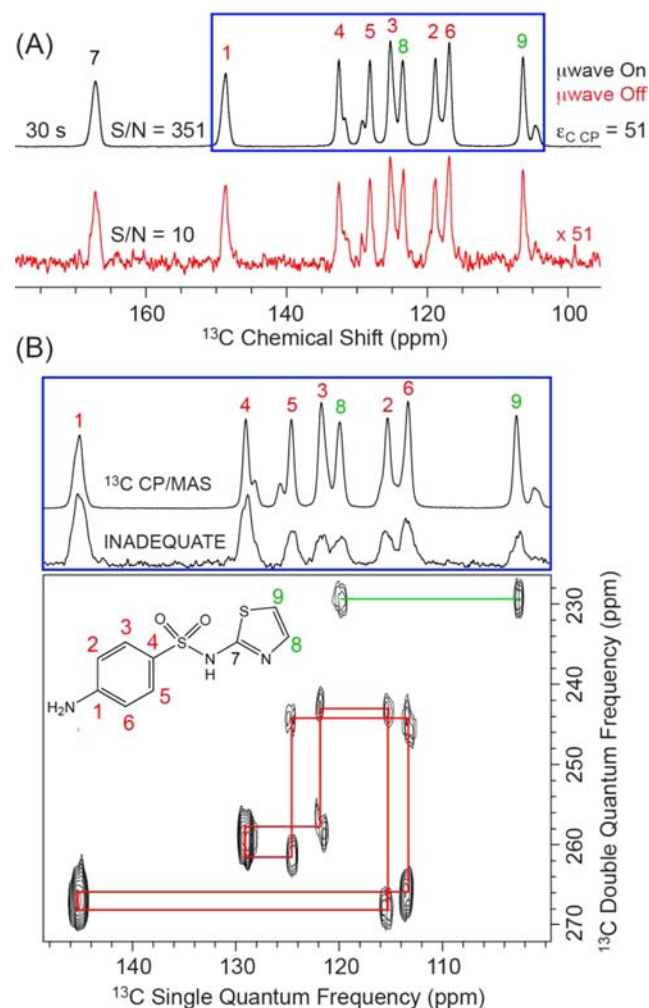


**Figure 6.** (A)  $^1\text{H}$ - $^{13}\text{C}$  CP/MAS solid-state NMR spectra of sulfathiazole impregnated with 16 mM bCTbK 1,3-dibromobutane solution. The  $\epsilon_{\text{CP}}$ , intensity scaling factor of the microwave off spectrum, and S/N ratio of each spectrum are provided. (B) 2D refocused INADEQUATE  $^{13}\text{C}$ - $^{13}\text{C}$  correlation spectrum of sulfathiazole acquired at natural isotopic abundance. A  $^{13}\text{C}$  CP/MAS spectrum is overlaid on top of the projection spectrum for comparison. The spectrum was acquired in a total experiment time of 16 h (30 s recycle delay, 30  $t_1$  increments, 64 scans per  $t_1$  increment, and  $\Delta t_1 = 80 \mu\text{s}$ ). A 4 ms delay was employed for generation of double quantum coherences. The molecular structure of sulfathiazole is shown and the carbon resonances are assigned. The connectivity of the carbon atoms is mapped out on the 2D spectrum.

of the results and observations from DNP experiments on sulfathiazole are similar to those made for glucose. While relaxation measurements of  $T_1(^1\text{H})$  were not performed for sulfathiazole, the value of  $\epsilon_{\text{CP}}$  was observed to be strongly dependent upon  $\tau$  (Figure S9, SI). With  $\epsilon_{\text{CP}}$  greater than 40, very high S/N spectra could be rapidly acquired and once again there appears to be no major loss in resolution at low temperatures. The large sensitivity gain provided by DNP again enabled the acquisition of a 2D refocused INADEQUATE in

only 16 h with natural  $^{13}\text{C}$  isotopic abundance (Figure 6B), yielding the complete carbon-13 assignment.

**DNP-Enhanced Solid-State NMR Spectra of a Microcrystalline Solid Characterized by a Short  $T_1(^1\text{H})$ .** DNP solid-state NMR experiments were performed on microcrystalline paracetamol (acetaminophen) to determine if this method is applicable to solids characterized by a short  $T_1(^1\text{H})$  (Figure 7). Paracetamol contains a methyl group and  $T_1(^1\text{H})$  is on the

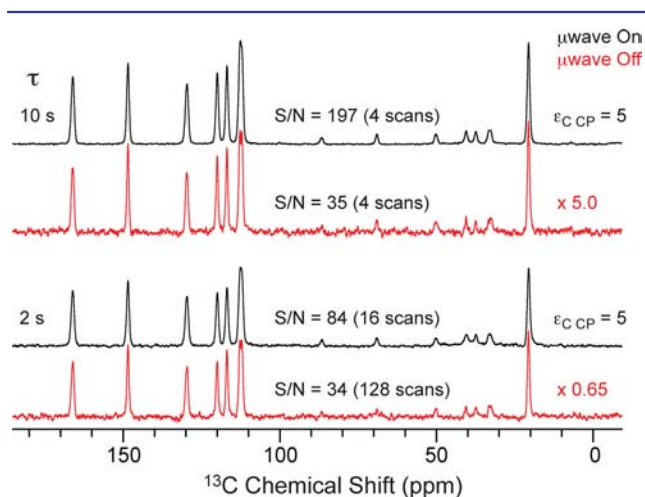


**Figure 7.**  $^1\text{H}$ – $^{13}\text{C}$  CP/MAS solid-state NMR spectra of paracetamol impregnated with 16 mM bCTbK 1,3-dibromobutane solution acquired with (black) and without (red) microwave irradiation. The  $\epsilon_{\text{CP}}$ , intensity scaling factor of the microwave off spectra, S/N, recycle delay, and number of scans acquired for each spectrum are provided. The low-intensity resonances between 100 ppm and 25 ppm are spinning sidebands or solvent resonances.

order of 2 s at room temperature. At 105 K for a sample impregnated with a 16 mM bCTbK  $\text{Br}_2\text{Bu}$  solution the relaxation data could be fit with a monoexponential function and  $T_1(^1\text{H})$  was measured to be 13.7(5) s (with DNP). An  $\epsilon_{\text{CP}}$  of 5 was obtained. As expected from the short value of  $T_1$  and our theoretical modeling, the value of  $\epsilon_{\text{CP}}$  is greatly reduced as compared to the  $\epsilon_{\text{CP}}$  for glucose and sulfathiazole. With eq 9 and assuming a  $T_{1,298\text{K}}$  of 2 s and a  $\Lambda$  ratio of 0.85,  $\Sigma^\dagger$  is calculated to be on the order of 5. In this case the thermal Boltzmann enhancement is largely offset by the increase in  $T_1(^1\text{H})$  at low temperatures. However, a sensitivity enhancement of 5 is still substantial, and will reduce experiment times by a factor of 25.

## CONCLUSIONS

DNP solid-state NMR provides sensitivity enhancements of 2 orders of magnitude for externally doped organic solids which possess a long  $T_1(^1\text{H})$ . This enables the rapid acquisition of natural abundance  $^{13}\text{C}$ – $^{13}\text{C}$  correlation spectra of unaltered solids. For the compounds examined here the high resolution of the room temperature  $^{13}\text{C}$  CP/MAS spectra is maintained so that there is a minimal trade off for the large increase in sensitivity. The method is also applicable to complexes characterized by shorter  $T_1(^1\text{H})$  such as paracetamol; however, the sensitivity enhancements are reduced. Provided  $T_1(^1\text{H})$  is relatively long,  $^1\text{H}$  spin diffusion can facilitate the transport of polarization over micrometer length scales, which demonstrates that the radicals do not need to be located in direct spatial proximity to the target nuclei to be polarized.

Microcrystalline samples were used here, but crystallinity is not a requirement (the essential feature is the grain size and a coupled network of abundant spins to transport polarization), and the method should be applicable to amorphous powders. We anticipate that this technique would also be very useful for examining formulations of pharmaceuticals where the active ingredient content is often in the range of 1–5 wt %. DNP experiments should also be useful for performing NMR experiments on organic solids with nuclei characterized by low receptivities (e.g.,  $^{14/15}\text{N}$ ,  $^{17}\text{O}$ ). Finally, it is hoped that this study will inspire new methods for doping systems with radicals for DNP.

## ASSOCIATED CONTENT

### Supporting Information

Details of NMR experiments, theoretical modeling, sample preparations, and additional NMR spectra. This material is available free of charge via the Internet at <http://pubs.acs.org>.

## AUTHOR INFORMATION

### Corresponding Author

lyndon.emsley@ens-lyon.fr

### Notes

The authors declare no competing financial interest.

## ACKNOWLEDGMENTS

Prof. Paul Tordo and Prof. Olivier Ouari (Aix-Marseille Université) are thanked for providing the bCTbK biradical. A.J.R. acknowledges support from a EU Marie-Curie IIF Fellowship (PIIF-GA-2010–274574). Financial support is acknowledged from the Agence Nationale de la Recherche grant ANR-2010-BLAN-0806-01, EQUIPEX contract ANR-10-EQPX-47-01, and the ETH Zürich. Drs. Moreno Lelli, Meghan Halse, and Maria Baias are thanked for stimulating discussions and assistance with solution NMR experiments. Drs. Marc A. Caporini and Melanie Rosay (Bruker USA) are thanked for assistance with the DNP solid-state NMR experiments. We are indebted to Drs. Werner E. Maas and Alain Belguise for providing access to the DNP solid-state NMR spectrometer.

## REFERENCES

- (1) Bryce, D. L.; Gee, M.; Wasylshen, R. E. *J. Phys. Chem. A* **2001**, *105*, 10413–10421.
- (2) Brown, S. P.; Spiess, H. W. *Chem. Rev.* **2001**, *101*, 4125–4155.
- (3) Bryce, D. L.; Sward, G. D.; Adiga, S. *J. Am. Chem. Soc.* **2006**, *128*, 2121–2134.
- (4) Harris, R. K. *Analyst* **2006**, *131*, 351–373.
- (5) Schaller, T.; Buchele, U. P.; Klarner, F. G.; Blaser, D.; Boese, R.; Brown, S. P.; Spiess, H. W.; Koziol, F.; Kussmann, J.; Ochsenfeld, C. *J. Am. Chem. Soc.* **2007**, *129*, 1293–1303.
- (6) Hamaed, H.; Pawlowski, J. M.; Cooper, B. F. T.; Fu, R.; Eichhorn, S. H.; Schurko, R. W. *J. Am. Chem. Soc.* **2008**, *130*, 11056–11065.
- (7) Vogt, F. G.; Clawson, J. S.; Strohmeier, M.; Edwards, A. J.; Pham, T. N.; Watson, S. A. *Cryst. Growth Des.* **2009**, *9*, 921–937.
- (8) Lee, D.; Struppe, J.; Elliott, D. W.; Mueller, L. J.; Titman, J. J. *Phys. Chem. Chem. Phys.* **2009**, *11*, 3547–3553.
- (9) Webber, A. L.; Elena, B.; Griffin, J. M.; Yates, J. R.; Pham, T. N.; Mauri, F.; Pickard, C. J.; Gil, A. M.; Stein, R.; Lesage, A.; Emsley, L.; Brown, S. P. *Phys. Chem. Chem. Phys.* **2010**, *12*, 6970–6983.
- (10) Iltot, A. J.; Palucha, S.; Batsanov, A. S.; Wilson, M. R.; Hodgkinson, P. *J. Am. Chem. Soc.* **2010**, *132*, 5179–5185.
- (11) Webber, A. L.; Masiero, S.; Pieraccini, S.; Burey, J. C.; Tatton, A. S.; Iuga, D.; Pham, T. N.; Spada, G. P.; Brown, S. P. *J. Am. Chem. Soc.* **2011**, *133*, 19777–19795.

- (12) O'Dell, L. A.; Schurko, R. W.; Harris, K. J.; Autschbach, J.; Ratcliffe, C. I. *J. Am. Chem. Soc.* **2011**, *133*, 527–546.
- (13) Tatton, A. S.; Pham, T. N.; Vogt, F. G.; Iuga, D.; Edwards, A. J.; Brown, S. P. *CrystEngComm* **2012**, *14*, 2654–2659.
- (14) Mafra, L.; Santos, S. M.; Siegel, R.; Alves, I.; Almeida Paz, F. A.; Dudenko, D.; Spiess, H. W. *J. Am. Chem. Soc.* **2012**, *134*, 71–74.
- (15) Dos, A.; Schimming, V.; Huot, M. C.; Limbach, H. H. *J. Am. Chem. Soc.* **2009**, *131*, 7641–7653.
- (16) Threlfall, T. L. *Analyst* **1995**, *120*, 2435–2460.
- (17) Harris, R. K. *Solid State Sci.* **2004**, *6*, 1025–1037.
- (18) Lubach, J. W.; Munson, E. J. In *Polymorphism*, 1st ed.; Hilfiker, R., Ed.; Wiley-VCH: Weinheim, Germany, 2006; pp 81–93.
- (19) Berendt, R. T.; Sperger, D. M.; Isbester, P. K.; Munson, E. J. *TrAC, Trends Anal. Chem.* **2006**, *25*, 977–984.
- (20) Griffin, J. M.; Martin, D. R.; Brown, S. P. *Angew. Chem., Int. Ed.* **2007**, *46*, 8036–8038.
- (21) Vogt, F. G. *Future Med. Chem.* **2010**, *2*, 915–921.
- (22) Ochsenfeld, C.; Brown, S. P.; Schnell, I.; Gauss, J.; Spiess, H. W. *J. Am. Chem. Soc.* **2001**, *123*, 2597–2606.
- (23) Taulelle, F. *Solid State Sci.* **2004**, *6*, 1053–1057.
- (24) Seidel, K.; Eitzkorn, M.; Sonnenberg, L.; Griesinger, C.; Sebald, A.; Baldus, M. *J. Phys. Chem. A* **2005**, *109*, 2436–2442.
- (25) Elena, B.; Emsley, L. *J. Am. Chem. Soc.* **2005**, *127*, 9140–9146.
- (26) Brouwer, D. H.; Darton, R. J.; Morris, R. E.; Levitt, M. H. *J. Am. Chem. Soc.* **2005**, *127*, 10365–10370.
- (27) Harris, R. K.; Hodgkinson, P.; Pickard, C. J.; Yates, J. R.; Zorin, V. *Magn. Reson. Chem.* **2007**, *45*, S174–S186.
- (28) Pickard, C. J.; Salager, E.; Pintacuda, G.; Elena, B.; Emsley, L. *J. Am. Chem. Soc.* **2007**, *129*, 8932–8933.
- (29) Salager, E.; Stein, R. S.; Pickard, C. J.; Elena, B.; Emsley, L. *Phys. Chem. Chem. Phys.* **2009**, *11*, 2610–2621.
- (30) Salager, E.; Day, G. M.; Stein, R. S.; Pickard, C. J.; Elena, B.; Emsley, L. *J. Am. Chem. Soc.* **2010**, *132*, 2564–2565.
- (31) Apperley, D. C.; Fletton, R. A.; Harris, R. K.; Lancaster, R. W.; Tavener, S.; Threlfall, T. L. *J. Pharm. Sci.* **1999**, *88*, 1275–1280.
- (32) Ganapathy, S.; Naito, A.; McDowell, C. A. *J. Am. Chem. Soc.* **1981**, *103*, 6011–6015.
- (33) Brown, C. E. *J. Am. Chem. Soc.* **1982**, *104*, 5608–5610.
- (34) Alemany, L. B.; Grant, D. M.; Pugmire, R. J.; Alger, T. D.; Zilm, K. W. *J. Am. Chem. Soc.* **1983**, *105*, 2133–2141.
- (35) Alemany, L. B.; Grant, D. M.; Pugmire, R. J.; Alger, T. D.; Zilm, K. W. *J. Am. Chem. Soc.* **1983**, *105*, 2142–2147.
- (36) Murray, D. P.; Dechter, J. J.; Kispert, L. D. *J. Polym. Sci., Part C: Polym. Lett.* **1984**, *22*, 519–522.
- (37) Nelson, B. N.; Schieber, L. J.; Barich, D. H.; Lubach, J. W.; Offerdahl, T. J.; Lewis, D. H.; Heinrich, J. P.; Munson, E. J. *Solid State Nucl. Magn. Reson.* **2006**, *29*, 204–213.
- (38) Ernst, R. R.; Bodenhausen, G.; Wokaun, A. In *Principles of Nuclear Magnetic Resonance in One and Two Dimensions*; 2nd ed.; Oxford University Press: Oxford, UK, 1987.
- (39) Bloembergen, N. *Physica* **1949**, *15*, 386–426.
- (40) Carver, T. R.; Slichter, C. P. *Phys. Rev.* **1953**, *92*, 212–213.
- (41) Overhauser, A. W. *Phys. Rev.* **1953**, *92*, 411–415.
- (42) Slichter, C. P. *Phys. Chem. Chem. Phys.* **2010**, *12*, 5741–5751.
- (43) Becerra, L. R.; Gerfen, G. J.; Temkin, R. J.; Singel, D. J.; Griffin, R. G. *Phys. Rev. Lett.* **1993**, *71*, 3561–3564.
- (44) Becerra, L. R.; Gerfen, G. J.; Bellew, B. F.; Bryant, J. A.; Hall, D. A.; Inati, S. J.; Weber, R. T.; Un, S.; Prisner, T. F.; McDermott, A. E.; Fishbein, K. W.; Kreisler, K. E.; Temkin, R. J.; Singel, D. J.; Griffin, R. G. *J. Magn. Reson., Ser. A* **1995**, *117*, 28–40.
- (45) Maly, T.; Debelouchina, G. T.; Bajaj, V. S.; Hu, K. N.; Joo, C. G.; Mak-Jurkauskas, M. L.; Sirigiri, J. R.; van der Wel, P. C. A.; Herzfeld, J.; Temkin, R. J.; Griffin, R. G. *J. Chem. Phys.* **2008**, *128*, 052211–052211–052219.
- (46) Hall, D. A.; Maus, D. C.; Gerfen, G. J.; Inati, S. J.; Becerra, L. R.; Dahlquist, F. W.; Griffin, R. G. *Science* **1997**, *276*, 930–932.
- (47) Hu, K. N.; Yu, H. H.; Swager, T. M.; Griffin, R. G. *J. Am. Chem. Soc.* **2004**, *126*, 10844–10845.
- (48) Song, C. S.; Hu, K. N.; Joo, C. G.; Swager, T. M.; Griffin, R. G. *J. Am. Chem. Soc.* **2006**, *128*, 11385–11390.
- (49) Matsuki, Y.; Maly, T.; Ouari, O.; Karoui, H.; Le Moigne, F.; Rizzato, E.; Lyubenova, S.; Herzfeld, J.; Prisner, T.; Tordo, P.; Griffin, R. G. *Angew. Chem., Int. Ed.* **2009**, *48*, 4996–5000.
- (50) Zagdoun, A.; Casano, G.; Ouari, O.; Lapadula, G.; Rossini, A. J.; Lelli, M.; Baffert, M.; Gajan, D.; Veyre, L.; Maas, W. E.; Rosay, M.; Weber, R. T.; Thieuleux, C.; Coperet, C.; Lesage, A.; Tordo, P.; Emsley, L. *J. Am. Chem. Soc.* **2012**, *134*, 2284–2291.
- (51) Dane, E. L.; Corzilius, B.; Rizzato, E.; Stocker, P.; Maly, T.; Smith, A. A.; Griffin, R. G.; Ouari, O.; Tordo, P.; Swager, T. M. *J. Org. Chem.* **2012**, *77*, 1789–1797.
- (52) Kiesewetter, M. K.; Corzilius, B.; Smith, A. A.; Griffin, R. G.; Swager, T. M. *J. Am. Chem. Soc.* **2012**, *134*, 4537–4540.
- (53) Rossini, A. J.; Zagdoun, A.; Lelli, M.; Gajan, D.; Rascon, F.; Rosay, M.; Maas, W. E.; Coperet, C.; Lesage, A.; Emsley, L. *Chem. Sci.* **2012**, *3*, 108–115.
- (54) van der Wel, P. C. A.; Hu, K. N.; Lewandowski, J.; Griffin, R. G. *J. Am. Chem. Soc.* **2006**, *128*, 10840–10846.
- (55) Bajaj, V. S.; Mak-Jurkauskas, M. L.; Belenky, M.; Herzfeld, J.; Griffin, R. G. *Proc. Natl. Acad. Sci. U.S.A.* **2009**, *106*, 9244–9249.
- (56) Salmikov, E.; Rosay, M.; Pawsey, S.; Ouari, O.; Tordo, P.; Bechinger, B. *J. Am. Chem. Soc.* **2010**, *132*, 5940–5941.
- (57) Akbey, U.; Franks, W. T.; Linden, A.; Lange, S.; Griffin, R. G.; van Rossum, B. J.; Oschkinat, H. *Angew. Chem., Int. Ed.* **2010**, *49*, 7803–7806.
- (58) Reggie, L.; Lopez, J. J.; Collinson, I.; Glaubitz, C.; Lorch, M. *J. Am. Chem. Soc.* **2011**, *133*, 19084–19086.
- (59) Linden, A. H.; Lange, S.; Franks, W. T.; Akbey, U.; Specker, E.; van Rossum, B.-J.; Oschkinat, H. *J. Am. Chem. Soc.* **2011**, *133*, 19266–19269.
- (60) Sergeev, I. V.; Day, L. A.; Goldbourt, A.; McDermott, A. E. *J. Am. Chem. Soc.* **2011**, *133*, 20208–20217.
- (61) Jacso, T.; Franks, W. T.; Rose, H.; Fink, U.; Broecker, J.; Keller, S.; Oschkinat, H.; Reif, B. *Angew. Chem., Int. Ed.* **2012**, *51*, 432–435.
- (62) Renault, M.; Pawsey, S.; Bos, M. P.; Koers, E. J.; Nand, D.; Tommassen-van Boxel, R.; Rosay, M.; Tommassen, J.; Maas, W. E.; Baldus, M. *Angew. Chem., Int. Ed.* **2012**, *51*, 2998–3001.
- (63) Maly, T.; Cui, D. T.; Griffin, R. G.; Miller, A. F. *J. Phys. Chem. B* **2012**, *116*, 7055–7065.
- (64) Lesage, A.; Lelli, M.; Gajan, D.; Caporini, M. A.; Vitzthum, V.; Mieville, P.; Alauzun, J.; Roussey, A.; Thieuleux, C.; Mehdi, A.; Bodenhausen, G.; Copéret, C.; Emsley, L. *J. Am. Chem. Soc.* **2010**, *132*, 15459–15461.
- (65) Lelli, M.; Gajan, D.; Lesage, A.; Caporini, M. A.; Vitzthum, V.; Mieville, P.; Heroguel, F.; Rascon, F.; Roussey, A.; Thieuleux, C.; Boualleg, M.; Veyre, L.; Bodenhausen, G.; Copéret, C.; Emsley, L. *J. Am. Chem. Soc.* **2011**, *133*, 2104–2107.
- (66) Zagdoun, A.; Rossini, A. J.; Gajan, D.; Bourdolle, A.; Ouari, O.; Rosay, M.; Maas, W. E.; Tordo, P.; Lelli, M.; Emsley, L.; Lesage, A.; Copéret, C. *Chem. Commun.* **2011**, *48*, 654–656.
- (67) Lafon, O.; Rosay, M.; Aussenac, F.; Lu, X.; Trebosc, J.; Cristini, O.; Kinowski, C.; Touati, N.; Vezin, H.; Amoureux, J. P. *Angew. Chem., Int. Ed.* **2011**, *50*, 8367–8370.
- (68) Rossini, A. J.; Zagdoun, A.; Lelli, M.; Canivet, J.; Aguado, S.; Ouari, O.; Tordo, P.; Rosay, M.; Maas, W. E.; Coperet, C.; Farrusseng, D.; Emsley, L.; Lesage, A. *Angew. Chem., Int. Ed.* **2012**, *51*, 123–127.
- (69) Vitzthum, V.; Mieville, P.; Carnevale, D.; Caporini, M. A.; Gajan, D.; Coperet, C.; Lelli, M.; Zagdoun, A.; Rossini, A. J.; Lesage, A.; Emsley, L.; Bodenhausen, G. *Chem. Commun.* **2012**, *48*, 1988–1990.
- (70) Lock, H.; Maciel, G. E.; Johnson, C. E. *J. Mater. Res.* **1992**, *7*, 2791–2797.
- (71) Wind, R. A.; Lewis, R.; Lock, H.; Maciel, G. E. *Adv. Chem. Ser.* **1993**, *45*–63.
- (72) Casabianca, L. B.; Shames, A. I.; Panich, A. M.; Shenderova, O.; Frydman, L. *J. Phys. Chem. C* **2011**, *115*, 19041–19048.
- (73) Lesage, A.; Bardet, M.; Emsley, L. *J. Am. Chem. Soc.* **1999**, *121*, 10987–10993.

- (74) Hohwy, M.; Jakobsen, H. J.; Eden, M.; Levitt, M. H.; Nielsen, N. *C. J. Chem. Phys.* **1998**, *108*, 2686–2694.
- (75) Rosay, M.; Tometich, L.; Pawsey, S.; Bader, R.; Schauwecker, R.; Blank, M.; Borchard, P. M.; Cauffman, S. R.; Felch, K. L.; Weber, R. T.; Temkin, R. J.; Griffin, R. G.; Maas, W. E. *Phys. Chem. Chem. Phys.* **2010**, *12*, 5850–5860.
- (76) Peersen, O.; Wu, X.; Kustanovich, I.; Smith, S. J. *Magn. Reson., Ser. A* **1993**, *104*, 334–339.
- (77) Fung, B. M.; Khitrin, A. K.; Ermolaev, K. J. *Magn. Reson.* **2000**, *142*, 97–101.
- (78) Horvitz, E. P. *Phys. Rev. B* **1971**, *3*, 2868–2872.
- (79) Leguennec, P.; Nechtschein, M.; Travers, J. P. *Phys. Rev. B* **1993**, *47*, 2893–2896.
- (80) Rabbani, S. R.; Edmonds, D. T. *Phys. Rev. B* **1994**, *50*, 6184–6188.
- (81) Brownstein, K. R.; Tarr, C. E. *Phys. Rev. A* **1979**, *19*, 2446–2453.
- (82) Weibull, W. J. *Appl. Mech.* **1951**, *18*, 293–297.
- (83) Rosin, P.; Rammler, E. J. *Inst. Fuel* **1933**, *7*, 29–36.
- (84) Linden, A. H.; Franks, W. T.; Akbey, U.; Lange, S.; van Rossum, B.-J.; Oschkinat, H. J. *Biomol. NMR* **2011**, *51*, 283–292.
- (85) Barnes, A. B.; Corzilius, B.; Mak-Jurkauskas, M. L.; Andreas, L. B.; Bajaj, V. S.; Matsuki, Y.; Belenky, M. L.; Lugtenburg, J.; Sirigiri, J. R.; Temkin, R. J.; Herzfeld, J.; Griffin, R. G. *Phys. Chem. Chem. Phys.* **2010**, *12*, 5861–5867.
- (86) Rabbani, S. R.; Mendonca, C.; Mamani, J. B.; Cervantes, H. *Braz. J. Phys.* **2006**, *36*, 28–33.
- (87) Lange, S.; Linden, A. H.; Akbey, U.; Franks, W. T.; Loening, N. M.; van Rossum, B.-J.; Oschkinat, H. J. *Magn. Reson.* **2012**, *216*, 209–212.
- (88) Vitzthum, V.; Borcard, F.; Jannin, S.; Morin, M.; Mieville, P.; Caporini, M. A.; Sienkiewicz, A.; Gerber-Lemaire, S.; Bodenhausen, G. *ChemPhysChem* **2011**, *12*, 2929–2932.
- (89) Lee, Y. K.; Kurur, N. D.; Helmle, M.; Johannessen, O. G.; Nielsen, N. C.; Levitt, M. H. *Chem. Phys. Lett.* **1995**, *242*, 304–309.
- (90) De Paepe, G.; Lesage, A.; Steuernagel, S.; Emsley, L. *ChemPhysChem* **2004**, *5*, 869–875.
- (91) Harris, R. K.; Cadars, S.; Emsley, L.; Yates, J. R.; Pickard, C. J.; Jetti, R. K. R.; Griesser, U. J. *Phys. Chem. Chem. Phys.* **2007**, *9*, 360–368.
- (92) Harris, R. K.; Joyce, S. A.; Pickard, C. J.; Cadars, S.; Emsley, L. *Phys. Chem. Chem. Phys.* **2006**, *8*, 137–143.
- (93) Both DNP experiments were performed approximately one week after those depicted in Figure 2. During this time the biradical solution was observed to degrade as indicated by a reduction in the DNP enhancement and increase in longitudinal relaxation observed for a second sample of ground glucose (Figure S7, SI). This suggests that the biradical was likely partially reduced by reaction with EtBr<sub>4</sub> over the course of the week. To control for this degradation, experiments were performed on a second sample of impregnated ground glucose that was prepared at the same time as the as-received sample. The solid-state NMR spectra were acquired within hours of one another.
- (94) Lubach, J. W.; Xu, D.; Segmuller, B. E.; Munson, E. J. *J. Pharm. Sci.* **2007**, *96*, 777–787.